

Multi-scale modelling of heterogeneous materials with fixed and evolving microstructures*

Jiun-Shyan Chen¹ and Shafiqh Mehraeen²

5731G Boelter Hall, Civil & Environmental Engineering Department, University of California, Los Angeles (UCLA), Los Angeles, CA 90095, USA

E-mail: jschen@seas.ucla.edu

Received 23 April 2004, in final form 26 April 2004

Published 8 December 2004

Online at stacks.iop.org/MSMSE/13/95

Abstract

Many engineering and scientific problems require a full understanding of physical phenomena that span a wide spectrum of spatial length scales. These multi-scale problems cannot be analysed readily under the classical continuum mechanics framework. While classical methods have been proposed to study the physical phenomena on smaller scales and the resulting information has been transferred by homogenization techniques onto larger scales, effective methods to explicitly couple information at multiple length scales are still lacking. Passing information between physical models at different length scales requires mathematically consistent and physically meaningful formulation and numerical techniques. This paper presents a class of multi-scale mathematical and computational formulations as well as homogenization and localization numerical procedures for multi-scale modelling of (1) materials with fixed microstructures, and (2) problems with evolving microstructures such as stressed grain growth processes in polycrystalline materials. Wavelet-based computational methods are introduced for multi-scale modelling and homogenization of materials with fixed microstructures. Two wavelet-based methods, the wavelet Galerkin method and wavelet projection method, are presented. For problems with evolving microstructures, a multi-scale variational formulation based on an asymptotic expansion method and a double-grid numerical method is proposed.

1. Introduction

Understanding the fundamental concepts by which materials microstructure and evolution control the behaviour of engineering materials has been one of the principal objectives

* Originally presented at the [USNCCM Conference on Multiscale Modelling and Simulation of Material Behaviour \(27–31 July 2003, Albuquerque, NM, USA\)](#)

¹ Author to whom any correspondence should be addressed.

² Graduate student.

in materials research. Co-existing coarse and fine scale features in this pursuit poses a considerable challenge in mathematical formulation and numerical solution procedures. Obtaining both effective computational methods capable of reconciling coarse and fine scale features and a reliable solution on the most essential scale is of critical importance to multi-scale problems. The objective of homogenization is to find the differential equation that the coarse scale solution satisfies and to construct the corresponding differential operator. In general, the multi-scale problem can be categorized into fixed and evolving microstructure classes, both of which require elaborate mathematical and computational techniques in order to proceed.

In the field of micromechanics, noteworthy homogenization theories have been introduced by Mura [35], Christensen [12] and Nemat-Nasar and Hori [38]. For linearly elastic heterogeneous solids, exact averaging theorems and several homogenization models have been introduced by Eshelby (1957), Hashin (1965) and Nemat-Nasser and Hori [36–39]. In the recent micromechanical approach by Nemat-Nasser, the bounds on the overall moduli of a broad class of composites with periodic microstructure were obtained by generalized Hashin–Shtrikman variational formulation principles [38]. An estimate of the overall moduli, based on the selection of the effective medium as the reference material, was then proposed for periodic microstructure [38].

The mathematical theory of homogenization for heterogeneous media also has been extensively developed by Babuska [2], Lions [5] and Duvant [19]. The homogenization frameworks have been applied to a variety of linear and nonlinear structural problems. Examples include the early work of homogenization in buckling analysis by Mignot *et al* [31], and homogenization incorporating Green's function and fast Fourier transform (FFT) approaches by Moulinec and Suquet [34]. In the asymptotic expansion approach [5], the relationship of macroscopic and microscopic solutions is obtained in the unit cell problem with periodicity. Through this relationship, the homogenized differential equation as well as the homogenized material property are obtained. Upon obtaining the coarse scale solution through the macroscopic problem, the fine scale solution is found through the coarse–fine scale solution relation. The asymptotic expansion approach also has been applied to homogenization of composites [21], the multi-grid based method [20] and multi-physics problems with multiple spatial and temporal scales [3, 5, 41, 46].

A hybrid micromechanics theory was introduced by Nemat-Nasser and Hori [24] to compare the physics-based average-field theory and the mathematical asymptotic-based homogenization theory. It was shown that they yield essentially the same effective moduli and homogenized boundary-value problems. Moreover, it was shown that the asymptotic-based homogenization theory can be applied to materials with a non-periodic microstructure and higher order effects can be accounted for [24]. Nonetheless, the asymptotic based methods necessitate the fine scale response to be well separated from the response on the coarser scales.

Alternatively, a multi-grid method for a periodic heterogeneous medium has been proposed [20, 25]. In this approach, an inter-grid transfer operator is constructed using asymptotic expansion so that the problem on the auxiliary grid gives rise to a homogenization problem. In this approach, a series of rapidly varying spatial scales are introduced to capture the effects of spatial fluctuations induced by spatial heterogeneities. Knapik [25] has also applied a Schur complement for a multi-grid based homogenization technique.

A multi-resolution approach [6, 7, 13, 16, 18] is another type of multi-scale method for problems with fixed microstructures. In multi-resolution analysis, the transition between two different scales is defined explicitly. In this approach, the reduction procedure is employed and repeated over several scales. Thus the method does not require coarse and fine scale solutions to be well separated [14]. In the context of multi-resolution analysis, a specific form of wavelets (Haar basis) has been employed under the Galerkin framework [1, 15, 22, 45]. This

wavelet Galerkin method entails representing the solution as an expansion of scaling functions at each scale. The multi-scale solution of the fine scale differential equation therefore is approximated by a truncated wavelet expansion as well as the scale decomposition of scaling functions and wavelets. By utilizing wavelet-like functions under the framework of the mesh-free method, a multi-resolution analysis has also been introduced to construct hierarchical coarse–fine scale decomposition [28, 29]. Note that the wavelet Galerkin method usually leads to integrals involving highly discontinuous derivatives of wavelets and scaling functions [26]. Thus the accurate evaluation of integrals of these derivatives plays a key role in the solution process.

The first part of this work introduces a wavelet Galerkin method utilizing the scale decomposition characteristics of wavelet functions for homogenization of heterogeneous material with fixed microstructure. With the linear orthogonal wavelet-based shape functions, the wavelet Galerkin method is enhanced by invoking the integration by parts to reduce the order of required differentiation and to yield a symmetric stiffness matrix. Moreover, natural boundary conditions can be introduced in the weak form. However, the wavelet Galerkin method requires the microstructure to match with the finest scale grid and thus creates complexity in heterogeneous media with irregular-shaped microstructures. To correct this limitation, a wavelet-based projection method is proposed in which the solution at the finest scale can be obtained by any numerical method. Consequently, the coarse scale solution is obtained by up-scaling using multi-scale wavelet functions.

Recently, application of multi-scale modelling to problems evolving microstructure has received much attention [33, 42, 43]. With problems involving microstructure evolution, wavelet-based methods that rely on fixed grid points to obtain the finest scale solution are inefficient. In the second part of this work, a multi-scale method capable of dealing with microstructure evolution is introduced for modelling of stressed grain growth. We first introduce asymptotic expansion of field variables in the variational equation to obtain the multi-scale grain structure evolution equations as well as the homogenized material properties of a grain network. A double-grid method is proposed to effectively model both moving discontinuities along the grain boundary and topological changes of the grain structures during grain growth processes.

The layout of this paper proceeds as follows. In section 2, wavelet-based methods for multi-scale modelling of material with fixed microstructure are presented. In section 3, a multi-scale variational formulation for modelling of material with evolving microstructure is introduced. Numerical procedures for multi-scale modelling of the stressed grain growth process are discussed in section 4. Concluding remarks are given in section 5.

2. Wavelet-based methods for multi-scale modelling of heterogeneous materials with fixed microstructures

2.1. Multi-scale wavelet Galerkin method

In the wavelet Galerkin method [1, 15, 40] both the test and the trial functions are selected to be wavelet basis functions. Since the standard wavelet Galerkin method for solving second-order differential equation contains integration of second-order derivatives of wavelets and scaling functions that are either highly oscillatory or even non-differentiable, the accurate evaluation of these integrals is a problematic issue confronting the solution process. In the proposed method, integration by parts is introduced to the weak form of the problem so that (1) the order of differentiation is reduced, (2) a symmetric stiffness matrix can be constructed and (3) the natural boundary conditions can be invoked in the weak form.

To clarify the idea, consider the following boundary value problem with \mathcal{L} the differential operator:

$$\begin{aligned} \mathcal{L}u &= f & \text{on } \Omega \\ u &= g & \text{on } \partial\Omega. \end{aligned} \quad (2.1)$$

The approximated solution $u(x)$ at scale $j + 1$, denoted as $u_{j+1}(x)$ in V_{j+1} , is expressed as

$$u(x) \approx u_{j+1}(x) = \bar{u}_j(x) + \tilde{u}_j(x). \quad (2.2)$$

Here, $\bar{u}_j(x)$ and $\tilde{u}_j(x)$ are the coarse and fine scale components of the scale j solution, respectively:

$$\begin{aligned} \bar{u}_j(x) &= \sum_k \bar{u}_k^j \phi_{j,k}^*(x) = \phi_j^{*\top} \bar{U}_j \\ \tilde{u}_j(x) &= \sum_k \tilde{u}_k^j \psi_{j,k}^*(x) = \psi_j^{*\top} \tilde{U}_j, \quad \bar{u}_j \in V_j, \quad \tilde{u}_j \in W_j, \end{aligned} \quad (2.3)$$

where

$$\begin{aligned} \bar{U}_j &= [\bar{u}_m^j \quad \bar{u}_{m+1}^j \quad \cdots \quad \bar{u}_{n-1}^j \quad \bar{u}_n^j]^\top \\ \tilde{U}_j &= [\tilde{u}_m^j \quad \tilde{u}_{m+1}^j \quad \cdots \quad \tilde{u}_{n-1}^j \quad \tilde{u}_n^j]^\top, \end{aligned} \quad (2.4)$$

$$\begin{aligned} \phi_j^* &= [\phi_{j,m}^* \quad \phi_{j,m+1}^* \quad \cdots \quad \phi_{j,n-1}^* \quad \phi_{j,n}^*]^\top \\ \psi_j^* &= [\psi_{j,m}^* \quad \psi_{j,m+1}^* \quad \cdots \quad \psi_{j,n-1}^* \quad \psi_{j,n}^*]^\top, \quad m < n, \quad m, n \in \mathbb{Z}, \end{aligned} \quad (2.5)$$

in which V_j and W_j are subspaces of an orthogonal scaling function and wavelet at scale j expanded by $\phi_{j,k}^*$ and $\psi_{j,k}^*$, respectively. The functions $\phi_{j,k}^*(x) = 2^{j/2} \phi^*(2^j x - n)$ and $\psi_{j,k}^* = 2^{j/2} \psi^*(2^j x - n)$ are orthogonal scaling function and wavelet used as the shape functions in the Galerkin framework (examples of linear scaling functions and wavelets are shown in figure 1), m and n are lower and upper limits of integer translation for orthogonal scaling functions and wavelets, and \bar{u}_m^j and \tilde{u}_m^j are unknown coefficients to be solved. Detailed definitions of scaling and wavelet function subspaces and construction of corresponding orthogonal scaling function and wavelet are given in appendix A. Using equations (2.3)–(2.5), one can rewrite equation (2.2) as

$$u(x) \approx u_{j+1}(x) = \varphi_{j+1}^\top U_{j+1}, \quad (2.6)$$

where

$$\begin{aligned} \varphi_{j+1} &= [\psi_j^{*\top} \quad \phi_j^{*\top}]^\top \\ U_{j+1} &= [\tilde{U}_j^\top \quad \bar{U}_j^\top]^\top. \end{aligned} \quad (2.7)$$

Next, the Galerkin approximation of problem (2.1) at scale $j + 1$ is expressed as

$$\begin{aligned} \langle \varphi_{j+1}, \mathcal{L}(\varphi_{j+1}^\top U_{j+1}) \rangle - \langle \varphi_{j+1}, f_{j+1} \rangle + \sum_{i=1}^{\text{NB}} \lambda_i [\varphi_{j+1}]_i &= 0 \\ [\varphi_{j+1}^\top]_i U_{j+1} &= g_i, \quad i = 1, \dots, \text{NB}, \end{aligned} \quad (2.8)$$

where

$$[\varphi_{j+1}^\top]_i = \varphi_{j+1}^\top|_{x_i \in \partial\Omega}. \quad (2.9)$$

Here λ_i are Lagrange multipliers to impose the essential boundary conditions, NB stands for the number of essential boundary conditions in the discretized fashion, and $\langle \cdot, \cdot \rangle$ denotes

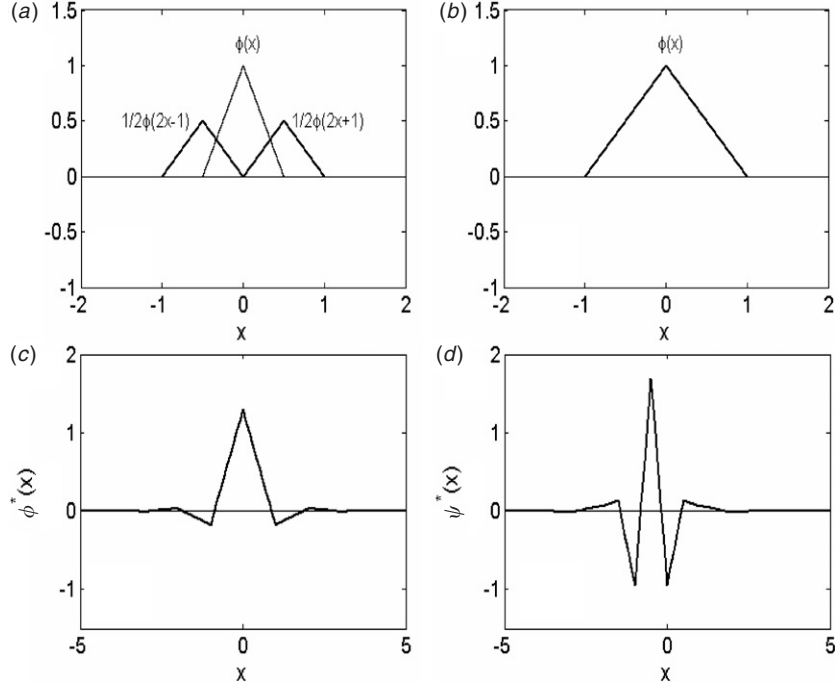


Figure 1. (a) Two-scale relation in hat function, (b) hat function, (c) orthogonal piecewise linear scaling function and (d) orthogonal piecewise linear wavelet.

the L^2 inner product between $L^2(\mathcal{R})$ functions. Upon introducing integration by parts in equation (2.8), the matrix form of the two-scale solution is obtained as:

$$\begin{bmatrix} \mathbf{K}_j^{\psi\psi} & \mathbf{K}_j^{\psi\phi} \\ \mathbf{K}_j^{\phi\psi} & \mathbf{K}_j^{\phi\phi} \\ \varphi_{j+1}^T|_{\partial\Omega} & [\mathbf{0}] \end{bmatrix} \begin{bmatrix} \tilde{\mathbf{U}}_j \\ \tilde{\mathbf{U}}_j \\ \lambda \end{bmatrix} = \begin{bmatrix} \mathbf{F}_j^\psi \\ \mathbf{F}_j^\phi \\ \mathbf{g} \end{bmatrix} \quad \text{or} \quad \mathbf{K}d = f, \quad (2.10)$$

where the stiffness submatrices $\mathbf{K}_j^{\phi\phi}$, $\mathbf{K}_j^{\phi\psi}$ and $\mathbf{K}_j^{\psi\psi}$ contain first-order derivatives of the scaling and wavelet functions and matrix λ contains Lagrange multipliers. Further, consider the following coarse–fine scale relationships of the scaling function and wavelet:

$$\phi^*(x) = \sum_k p_k \phi^*(2x - k), \quad \psi^*(x) = \sum_k q_k \phi^*(2x - k), \quad (2.11)$$

$$\phi^*(2x - l) = \sum_k [a_{l-2k} \phi^*(x - k) + b_{l-2k} \psi^*(x - k)], \quad l \in \mathbb{Z}. \quad (2.12)$$

Substituting equations (2.11) and (2.12) into equation (2.3), the fine scale j solution \bar{u}_l^j can be decomposed into scaling and wavelet components of the next coarser scale $j - 1$:

$$\bar{u}_k^{j-1} = \sum_l a_{l-2k} \bar{u}_l^j, \quad \tilde{u}_k^{j-1} = \sum_l b_{l-2k} \bar{u}_l^j. \quad (2.13)$$

Similarly, a fine scale solution can be reconstructed from the coarse scale solution by

$$\bar{u}_k^j = \sum_l [p_{k-2l} \bar{u}_l^{j-1} + q_{k-2l} \tilde{u}_l^{j-1}]. \quad (2.14)$$

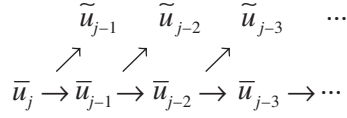


Figure 2. Decomposition algorithm.

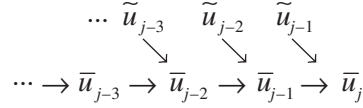


Figure 3. Reconstruction algorithm.

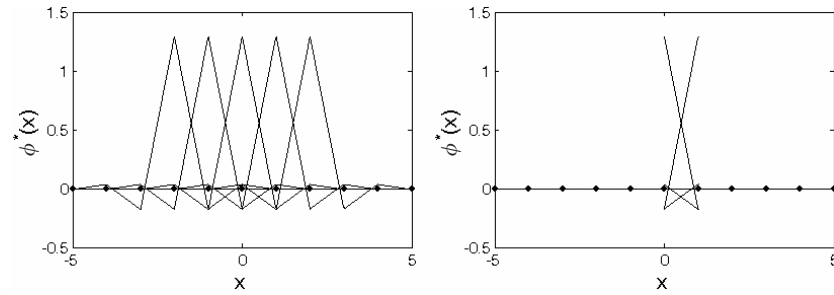


Figure 4. Dependence of the shape functions between two discrete points.

The decomposition and reconstruction algorithms are depicted in figures 2 and 3, respectively. A major difficulty involved in the solution of the discrete equation in equation (2.10) is the singularity of the stiffness matrix due to the dependency of the shape functions at any sub-domain between two given discrete points when linear scaling function and wavelet are used. As illustrated in figure 4, any interval between two discrete points is covered by four linearly independent functions. To resolve this problem, the eigenvalue shifting method is proposed below.

The improper zero eigenvalues in the discrete wavelet Galerkin equations are shifted to non-zero values without affecting the non-zero eigenvalues and the corresponding eigenvectors. It is noted that the improper nullity of the stiffness matrix can be removed without affecting the physical solution of the original problem if the force vector is in the range of the stiffness matrix. To clarify this, let \mathbf{K} be the $n \times n$ stiffness matrix. Eigenvector expansion of \mathbf{K} reads

$$\mathbf{K} = \sum_{i=m+1}^n \alpha_i \varphi_i \varphi_i^T, \quad (2.15)$$

where α_i are non-zero eigenvalues and φ_i are the corresponding eigenvectors. The eigenvectors $\{\varphi_i\}_{i=1}^m$ corresponding to zero eigenvalues can be eliminated by modifying the stiffness matrix as the following:

$$\bar{\mathbf{K}} = \sum_{i=1}^m \eta_i \varphi_i \varphi_i^T + \mathbf{K} = \sum_{i=1}^m \eta_i \varphi_i \varphi_i^T + \sum_{i=m+1}^n \alpha_i \varphi_i \varphi_i^T = \sum_{i=1}^n \bar{\alpha}_i \varphi_i \varphi_i^T, \quad (2.16)$$

where η_i are small positive numbers. From the above equation, it is obvious that the new matrix $\bar{\mathbf{K}}$ has exactly the same eigenvalues and eigenvectors except that zero eigenvalues have been shifted to η_i . Using eigenvector expansion with modified $\bar{\mathbf{K}}$ in replacing \mathbf{K} in equation (2.16), the solution of a linear system $\bar{\mathbf{K}}\bar{\mathbf{d}} = \mathbf{f}$ of equation (2.10) is

$$\left(\sum_{i=1}^n \bar{\alpha}_i \varphi_i \varphi_i^T \right) \left(\sum_{j=1}^n \bar{\beta}_j \varphi_j \right) = \mathbf{f}. \quad (2.17)$$

Using the orthonormality conditions of $\{\phi_i\}_{i=1}^n$, we obtain the solution

$$\begin{aligned} \bar{\beta}_j &= \frac{1}{\bar{\alpha}_j} \varphi_j \cdot \mathbf{f} = \frac{1}{\eta_j} \varphi_j \cdot \mathbf{f} = 0 & \text{for } j = 1 \sim m \\ \bar{\beta}_j &= \frac{1}{\bar{\alpha}_j} \varphi_j \cdot \mathbf{f} = \frac{1}{\alpha_j} \varphi_j \cdot \mathbf{f} & \text{for } j = m+1 \sim n. \end{aligned} \quad (2.18)$$

Thus, from equations (2.17) and (2.18), it is clear that the mode-shifting method applied in equation (2.17) suppresses the improper nullity without altering the non-rigid body solutions of the original problem in equation (2.10).

Once the solution $\mathbf{U}_{j+1} = [\tilde{\mathbf{U}}_j^T \quad \bar{\mathbf{U}}_j^T]^T$ at scale $j+1$ is obtained by means of the above-mentioned mode-shifting method, decomposition of the solution to obtain high and low scale components of any coarser scales $m < j$ can be cast via the wavelet transformation matrix \mathbf{w}_m . By introducing the discrete transformation operators \mathbf{P}_m and \mathbf{Q}_m , the transformation matrix \mathbf{w}_m takes the form of

$$\mathbf{w}_m = \begin{bmatrix} \mathbf{Q}_m \\ \mathbf{P}_m \end{bmatrix}, \quad \text{where } \begin{cases} \mathbf{Q}_m : V_{m+1} \rightarrow W_m \\ \mathbf{P}_m : V_{m+1} \rightarrow V_m, \end{cases} \quad (2.19)$$

where the operator \mathbf{Q}_m relates scaling function of scale $m+1$ to wavelet functions at scale m , and the operator \mathbf{P}_m transfers scaling function of scale $m+1$ to a scaling function corresponding to the next coarser level m . Upon construction of the discrete transformation operators \mathbf{P}_m and \mathbf{Q}_m , the transformation matrix \mathbf{w}_m for the Haar basis, and the linear orthogonal scaling function and wavelet have been obtained in [11] and are summarized in appendix B. Hence, at any scale $m < j$, scale decomposition can be obtained as

$$\mathbf{w}_m \mathbf{U}_{m+1}^1 = \begin{bmatrix} \mathbf{Q}_m \\ \mathbf{P}_m \end{bmatrix} \mathbf{U}_{m+1}^1 = \begin{bmatrix} \mathbf{U}_m^h \\ \mathbf{U}_m^l \end{bmatrix}. \quad (2.20)$$

Here, for notational convenience, the superscripts h and l denote high and low scale components, respectively, i.e. $\mathbf{U}_m^h = \tilde{\mathbf{U}}_m$, $\mathbf{U}_m^l = \bar{\mathbf{U}}_m$ with $\tilde{\mathbf{U}}_m$ and $\bar{\mathbf{U}}_m$ defined in equations (2.3) and (2.4). This procedure can be employed to yield the low and high scale components of the solution at any desired scale. Conversely, the finer scale solution at scale $n+1$ can be obtained via an inverse operation on the coarser scale solution at scale n by

$$\mathbf{U}_{n+1}^1 = \mathbf{w}_n^{-1} \begin{bmatrix} \mathbf{U}_n^h \\ \mathbf{U}_n^l \end{bmatrix}, \quad (2.21)$$

and \mathbf{U}_{n+1}^h can be obtained through a static condensation of the scale $n+1$ discrete equation in equation (2.10).

2.2. Multi-scale wavelet projection method

The wavelet Galerkin method discussed in section 2.1 requires a uniform grid on the finest scale. This results in complexity in multi-dimensional heterogeneous media which contain irregular-shaped microstructures. The interfaces between non-uniform microstructures cannot

be properly discretized using uniformly spaced wavelet basis functions. In this section a wavelet-based multi-scale projection method [30] is introduced as a simplification of the previously discussed wavelet Galerkin method.

Let the discrete form of the boundary value problem be expressed by [7]

$$\mathbf{L}U = \mathbf{F}, \quad (2.22)$$

where \mathbf{L} is a bounded linear operator. Let the above discrete equation be formed in the space V_{j+1} , i.e.

$$\mathbf{L}_{j+1}U_{j+1} = \mathbf{F}_{j+1} \quad \text{where } U_{j+1} \simeq U_{j+1}^1, \quad (2.23)$$

where subscripts denote the level of scale. Note that at the finest scale $j + 1$, the high scale component U_{j+1}^h is ignorable compared to the corresponding low scale component U_{j+1}^1 . Note that in this approach the highest scale solution U_{j+1} can be obtained by any numerical method. Consider the discrete projecting operators P_j and Q_j defined in equation (2.19). High and low scale components of scale j solution can be extracted as

$$U_j^1 = P_j U_{j+1}, \quad U_j^1 \in V_j, \quad U_{j+1} \in V_{j+1}, \quad (2.24)$$

$$U_j^h = Q_j U_{j+1}, \quad U_j^h \in W_j, \quad (2.25)$$

where function U_{j+1} is split into U_j^1 and U_j^h . By using the wavelet transformation operator w_j defined in equation (2.19), equation (2.23) can be transformed as

$$(w_j \mathbf{L}_{j+1} w_j^{-1})(w_j U_{j+1}) = \begin{bmatrix} \mathbf{L}_{11} & \mathbf{L}_{12} \\ \mathbf{L}_{21} & \mathbf{L}_{22} \end{bmatrix}_{j+1} \begin{bmatrix} U_j^h \\ U_j^1 \end{bmatrix} = w_j \mathbf{F}_{j+1} = \begin{bmatrix} \mathbf{F}_j^h \\ \mathbf{F}_j^1 \end{bmatrix}. \quad (2.26)$$

Here the low scale component U_j^1 is obtained by the Schur complement of \mathbf{L}_{22} in equation (2.26):

$$(\mathbf{L}_{22} - \mathbf{L}_{21} \mathbf{L}_{11}^{-1} \mathbf{L}_{12})_{j+1} U_j^1 = \mathbf{F}_j^1 - (\mathbf{L}_{21} \mathbf{L}_{11}^{-1})_{j+1} \mathbf{F}_j^h, \quad (2.27)$$

in which the Schur complement is defined as

$$\bar{\mathbf{L}}_{j+1} = (\mathbf{L}_{22} - \mathbf{L}_{21} \mathbf{L}_{11}^{-1} \mathbf{L}_{12})_{j+1}. \quad (2.28)$$

Here $\bar{\mathbf{L}}_{j+1}$ is the coarse scale operator, or so called the one-step reduction of the operator \mathbf{L}_{j+1} .

A multi-scale homogenization now is performed by first solving the solution at the finest scale. The low and high scale components of the next coarser levels then can be calculated by recursively performing the wavelet projections in equations (2.24) and (2.25). By contrast, localization, a reverse process of homogenization, is an operation in which the fine scale component at each scale is recovered by backward substitution of the coarse scale solution, i.e.

$$(\mathbf{L}_{11})_{j+1} U_j^h = \mathbf{F}_j^h - (\mathbf{L}_{12})_{j+1} U_j^1 \quad (2.29)$$

and the low scale solution of the next finest scale is obtained by

$$U_{j+1}^1 = w_j^{-1} \begin{bmatrix} U_j^h \\ U_j^1 \end{bmatrix}. \quad (2.30)$$

By repeating these two operations, the solution of any finer scale can be reconstructed hierarchically as illustrated in figure 5. These methods of homogenization and localization can be extended easily to higher dimensions.

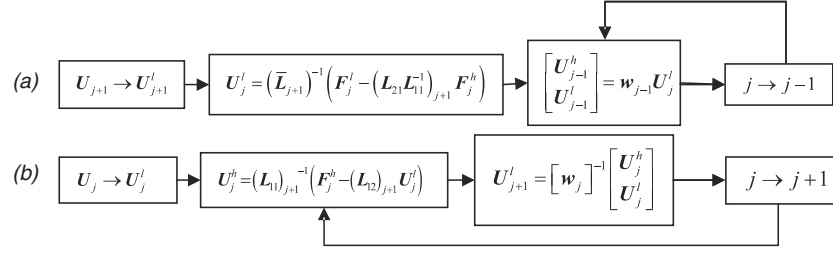


Figure 5. (a) Homogenization and (b) localization processes.

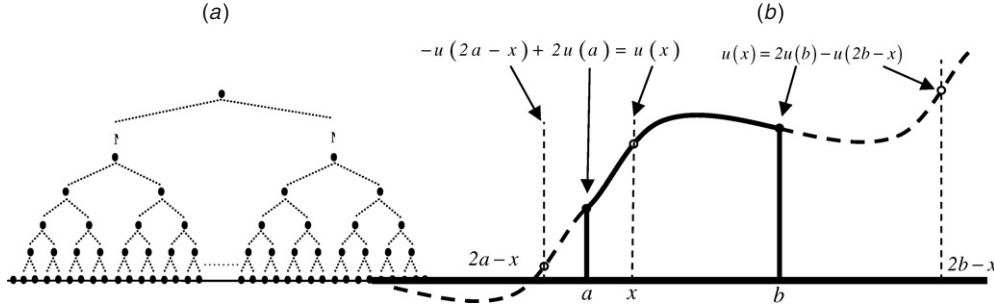


Figure 6. (a) Data compactness through the reduction process of wavelet-based homogenization; (b) Mirror image data construction in the fictitious domain (a and b : boundaries of real domain).

2.3. Numerical example

During the multi-scale homogenization calculation, shown in figure 6(a), at the coarser levels we observe fewer data points with respect to the finer levels. This is due to the fact that information at each coarse scale node is provided by some adjacent points at the finer scale. If no information is provided for the points outside of the domain, the zero coefficients associated with the representative data points outside the domain of response will pollute the whole solution after a few steps of the homogenization process. The proposed remedy for this problem is a mirror image technique that extends the physical domain with solution data to a fictitious domain with anti-symmetric data as shown in figure 6(b). With this mirror image process, the average of solution at the boundaries remains unchanged. Hence, this process does not generate any projection onto the wavelet spaces, since the wavelet projection filters out the deviation from the average.

In this problem, since the wavelet projection method produces almost identical results as that obtained by the wavelet Galerkin method, only the solutions of the wavelet Galerkin method are presented. To demonstrate the efficiency of the proposed wavelet Galerkin homogenization, consider the following elasticity problem with boundary conditions:

$$\frac{d}{dx} \left(E(x) \frac{du(x)}{dx} \right) = 0, \quad x \in]0, 5[\quad (2.31)$$

$$u(0) = 10, \quad u(5) = -10,$$

where a highly oscillating coefficient $E(x)$ as shown in figure 7 is used. To capture the fine scale details, the finest grid is set at $j = 7$, i.e. 2^7 discrete points are used. We employ linear

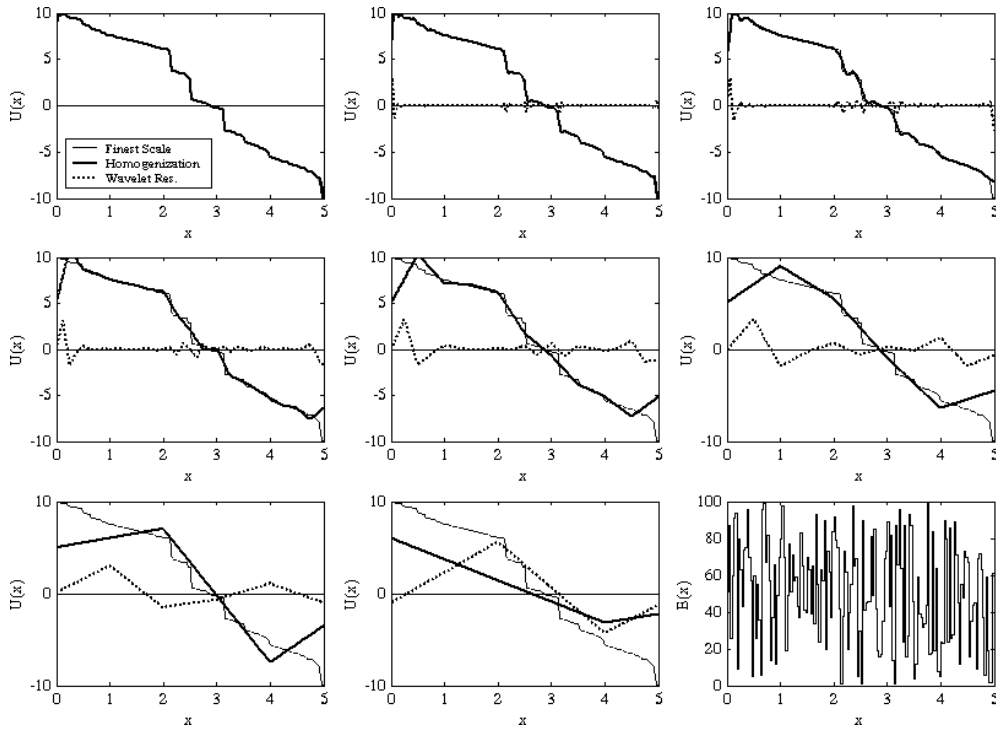


Figure 7. Lack of accuracy at the boundaries in multiple scales in wavelet Galerkin-based homogenization using linear orthogonal scaling function and wavelet without using mirror image technique from the upper left corner moving to the right: $j = 7, j = 6, j = 5, j = 4, j = 3, j = 2, j = 1, j = 0$, (j : level of resolution, $(E(x)u'(x))' = 0, u(0) = 10, u(5) = -10$).

orthogonal scaling and wavelet functions as illustrated in figures 1(c) and (d), since the Haar basis cannot be applied in the wavelet Galerkin method due to its nature of discontinuity. Homogenization starts from the fine scale $j = 7$ as shown in figure 7. Without the use of the mirror image technique, boundary conditions cannot be preserved accurately, thus oscillations occur due to unknown information inherent with the external shape functions covering the outside of problem domain. As homogenization proceeds, the oscillation initiated near the boundaries at the finer scales propagates to the interior of the problem domain at the coarser scales as shown in figure 7. To correct this deficiency, the mirror image technique is employed to enhance the solution and to remove the oscillation shown in figure 8. In each scale, the number of grid points is decreased by half. At the coarsest scale of $j = 0$, the homogenized solution yields a constant Young's modulus.

In the previous case, the Dirichlet boundaries were imposed at both ends of the problem domain, and the mirror image technique performed quite well. To identify the applicability of the mirror image method to Neumann-type boundary conditions, in this example we consider mixed Dirichlet and Neumann boundary conditions:

$$u(0) = 10, \quad u'(5) = -1. \quad (2.32)$$

The results shown in figure 9 are again satisfactory. This example also demonstrates that the multi-scale wavelet-based homogenization method is applicable even if the material property is not periodic.

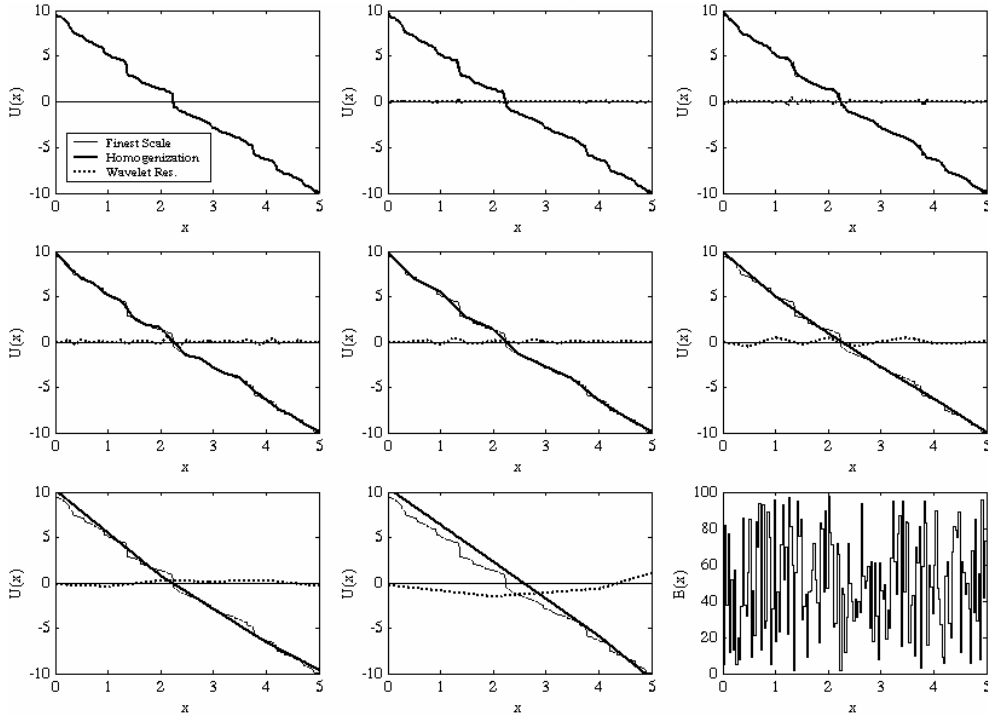


Figure 8. Wavelet Galerkin-based homogenization over multiple scales enhanced by the mirror image technique $j = 3, j = 2, j = 1, j = 0$, (j : level of resolution, $(E(x)u'(x))'$, $u(0) = 10, u(5) = -10$).

3. Multi-scale modelling of microstructural evolution

It was shown in section 2 that wavelet-based methods are effective in multi-scale homogenization of highly heterogeneous material with fixed heterogeneity. In the case where the microstructures are evolving, the wavelet-based multi-scale methods become ineffective in dealing with the moving material interfaces. In this section, we introduce a multi-scale variational formulation based on asymptotic expansion and the principle of virtual power, in conjunction with a double-grid numerical method, for modelling and homogenization of stressed grain growth that involves microstructure evolution. The expanded variational equation gives rise to multi-scale Euler equations describing evolution processes at different scales, the scale coupling relation, as well as the homogenized material properties. A stressed grain growth example is demonstrated using the proposed method.

3.1. Basic equations

The multi-scale hierarchy from a macro-scale continuum to a meso-scale grain network of polycrystalline material under consideration is shown in figure 10.

Let x be the macro-scale coordinate system in the physical domain. A unit cell with domain Ω and boundary Γ of a continuum in the physical domain is mapped to referential domain Ω^y and boundary Γ^y measured by a meso-scale coordinate y . The macro- and meso-scale coordinates are related through a scaling parameter λ by

$$dy_i = \frac{dx_i}{\lambda} \quad (3.1)$$

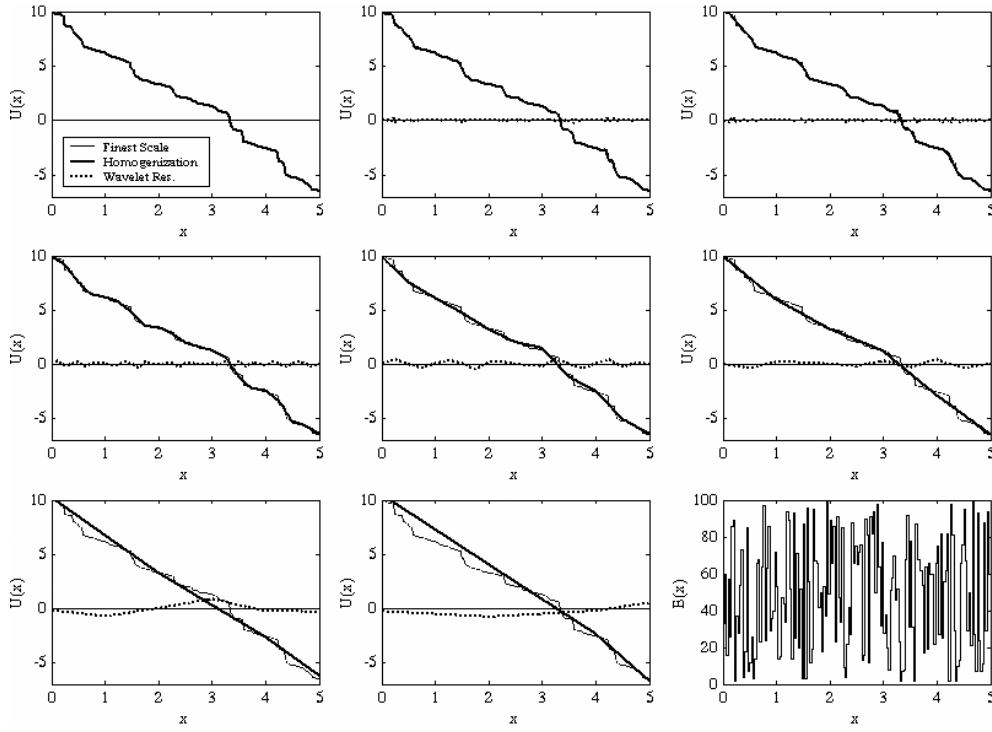


Figure 9. Accuracy healing at the boundaries in multiple scales in wavelet Galerkin-based homogenization using linear orthogonal scaling function and wavelet enhanced by mirror image technique from the upper left corner moving to the right: $j = 7, j = 6, j = 5, j = 4, j = 3, j = 2, j = 1, j = 0$, (j : level of resolution, $(E(x)u'(x))', u(0) = 10, u'(5) = -1$).

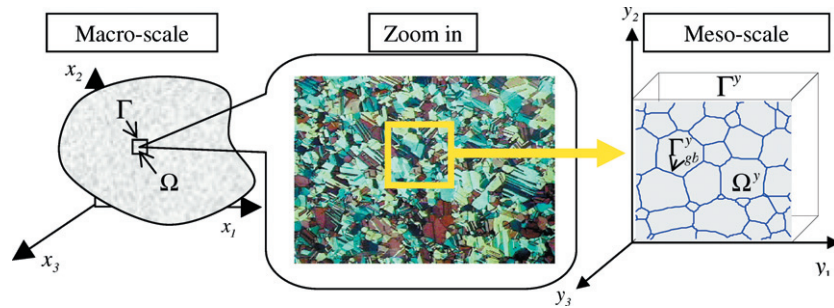


Figure 10. Length scale hierarchy of continuum and grain network.
(This figure is in colour only in the electronic version)

where λ is a very small real number. As shown in figure 11, a unit cell of a stressed grain network in the physical domain subjected to a surface traction \mathbf{h} on boundary Γ_h is considered. The grain boundaries in the unit cell are denoted as Γ_{gb} .

A variational equation for stressed grain growth based on the principle of virtual power described in the x -coordinate (Chen *et al* [9]) is

$$\delta \Pi(v, \bar{v}) = \delta \Pi_e(v) + \delta \Pi_{gb}(v, \bar{v}) = 0, \tag{3.2}$$

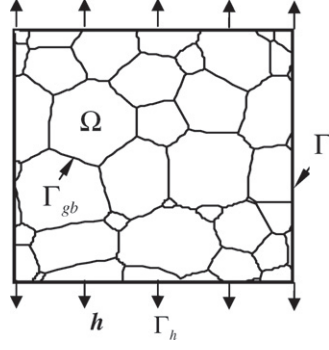


Figure 11. Unit cell structure of stressed grain network.

$$\delta \Pi_e(v) = \int_{\Omega} \frac{1}{2} \delta(\boldsymbol{\sigma} : \dot{\boldsymbol{\varepsilon}}) d\Omega - \int_{\Gamma_h} \delta \mathbf{v} \cdot \mathbf{h} d\Gamma - \int_{\Omega} \delta \mathbf{v} \cdot \mathbf{b} d\Omega, \quad (3.3)$$

$$\delta \Pi_{gb}(v, \bar{\mathbf{v}}) = \int_{\Gamma_{gb}} \frac{1}{2} (\boldsymbol{\sigma}^+ : \boldsymbol{\varepsilon}^+ - \boldsymbol{\sigma}^- : \boldsymbol{\varepsilon}^-) \delta \bar{v}_n d\Gamma + \int_{\Gamma_{gb}} \gamma \left(\frac{\partial \delta \bar{v}_s}{\partial s} + \frac{\delta \bar{v}_n}{R} \right) d\Gamma + \int_{\Gamma_{gb}} \frac{\delta \bar{v}_n}{\mu} \bar{v}_n d\Gamma, \quad (3.4)$$

where $\delta \Pi_e$ is the virtual power associated with grain deformation, $\delta \Pi_{gb}$ is the virtual power associated with driving forces acting on grain boundaries, \mathbf{v} is the grain material velocity, $\bar{\mathbf{v}}$ is the grain boundary migration velocity, \bar{v}_n is the normal velocity pointing away from the centre of curvature of the grain boundary, \bar{v}_s is the tangential velocity along the grain boundary, γ is the surface tension (the boundary energy per unit area), R is the radius of curvature of the grain boundary, μ is the mobility representing the ease with which the grain boundary can migrate, \mathbf{h} is the surface traction applied on the traction boundary Γ_h , \mathbf{b} is body force, $\boldsymbol{\sigma}^+$ and $\boldsymbol{\varepsilon}^+$, respectively, are the stress and strain in the grain that gains virtual area $\delta \bar{v}_n d\Gamma$ (grain A), and $\boldsymbol{\sigma}^-$ and $\boldsymbol{\varepsilon}^-$, respectively, are the stress and strain in the grain located on the other side of the boundary (grain B), as shown in figure 12. Detailed discussions of this can be found in [10]. We assume the stress–strain relation follows an anisotropic creep law:

$$\sigma_{ij} = C_{ijkl} \dot{\varepsilon}_{kl}. \quad (3.5)$$

To describe multi-scale material behaviour, the material velocity \mathbf{v} is expressed in the asymptotic expansion form [5]

$$v_i(\mathbf{x}, \mathbf{y}) = v_i^{[0]}(\mathbf{x}, \mathbf{y}) + \lambda v_i^{[1]}(\mathbf{x}, \mathbf{y}) + O(\lambda^2), \quad (3.6)$$

where $v_i^{[0]}$ and $v_i^{[1]}$ are macro- (coarse) scale and meso- (fine) scale components of material velocity, respectively, and the superscript $[n]$ denotes the level of scale. For a function expressed in both coarse and fine scale coordinates, the following relationship holds:

$$\frac{\partial}{\partial x_i} = \frac{\partial}{\partial x_i} \Big|_{[y]} + \frac{\partial}{\partial y_i} \Big|_{[x]} \frac{\partial y_i}{\partial x_i} = \frac{\partial}{\partial x_i} \Big|_{[y]} + \frac{1}{\lambda} \frac{\partial}{\partial y_i} \Big|_{[x]}. \quad (3.7)$$

For notational simplicity, the subscripts $[x]$ and $[y]$ are dropped hereafter. Following the chain rule in equation (3.7), the strain rate $\dot{\varepsilon}_{ij}$ is expressed as

$$\dot{\varepsilon}_{ij} = \lambda^{-1} \dot{\varepsilon}_{ij}^{[-1]} + \dot{\varepsilon}_{ij}^{[0]} + \lambda \dot{\varepsilon}_{ij}^{[1]} + \lambda^2 \dot{\varepsilon}_{ij}^{[2]} + \dots, \quad (3.8)$$

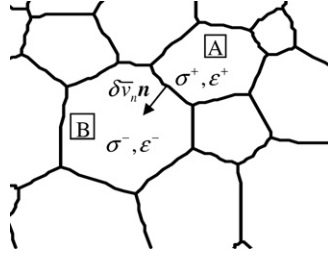


Figure 12. Strain energy change due to grain boundary migration.

where

$$\dot{\varepsilon}_{ij}^{[-1]} = \dot{\varepsilon}_{ij}^{[0]} = \frac{1}{2} \left(\frac{\partial v_i^{[0]}}{\partial y_j} + \frac{\partial v_j^{[0]}}{\partial y_i} \right), \quad \dot{\varepsilon}_{ij}^{[k]} = (\dot{\varepsilon}_{ij}^{[k]} + \dot{\varepsilon}_{ij}^{[k+1]}), \quad \forall k \geq 0, \quad k \in \mathbb{Z} \quad (3.9)$$

and

$$\dot{\varepsilon}_{ij}^{[k]} = \frac{1}{2} \left(\frac{\partial v_i^{[k]}}{\partial x_j} + \frac{\partial v_j^{[k]}}{\partial x_i} \right), \quad \dot{\varepsilon}_{ij}^{[k]} = \frac{1}{2} \left(\frac{\partial v_i^{[k]}}{\partial y_j} + \frac{\partial v_j^{[k]}}{\partial y_i} \right). \quad (3.10)$$

The expansion of stress field is obtained by using creep law:

$$\sigma_{ij} = \lambda^{-1} \sigma_{ij}^{[-1]} + \sigma_{ij}^{[0]} + \lambda \sigma_{ij}^{[1]} + \lambda^2 \sigma_{ij}^{[2]} + \dots, \quad (3.11)$$

where

$$\sigma_{ij}^{[k]} = C_{ijkl} \dot{\varepsilon}_{kl}^{[k]}. \quad (3.12)$$

3.2. Multi-scale variational formulation

The variational formulation can be decomposed hierarchically into its coarse and fine scale components by applying asymptotic expansions to material velocities, strain rates and stress in equation (3.2). In this section, the multi-scale Euler equations (strong forms) representing grain structure equilibrium and grain boundary evolution equations will be derived. Taking the asymptotic expansion of field variables, the total virtual power takes the form of [10]

$$\delta \Pi(\mathbf{v}^{[0]} + \lambda \mathbf{v}^{[1]}, \bar{\mathbf{v}}) = \lambda^{-2} \delta \Pi_e^{[-2]} + \lambda^{-1} \delta \Pi_e^{[-1]} + \delta \Pi^{[0]} + O(\lambda) = 0. \quad (3.13)$$

As λ approaches zero, equation (3.13) leads to

$$I_1 = \delta \Pi_e^{[-2]}(\mathbf{v}) = \int_{\Omega} \frac{1}{2} \delta(\dot{\varepsilon}_{ij}^{[-1]} \sigma_{ij}^{[-1]}) d\Omega = 0, \quad (3.14)$$

$$I_2 = \delta \Pi_e^{[-1]}(\mathbf{v}) = \int_{\Omega} \frac{1}{2} \delta(\dot{\varepsilon}_{ij}^{[-1]} \sigma_{ij}^{[0]} + \dot{\varepsilon}_{ij}^{[0]} \sigma_{ij}^{[-1]}) d\Omega = 0, \quad (3.15)$$

as well as $\delta \Pi^{[0]} = \delta \Pi_e^{[0]}(\mathbf{v}) + \delta \Pi_{gb}(\mathbf{v}, \bar{\mathbf{v}}) = 0$, which yields

$$\begin{aligned} I_3 = \delta \Pi_e^{[0]}(\mathbf{v}) &= \int_{\Omega} \frac{1}{2} \delta(\dot{\varepsilon}_{ij}^{[-1]} \sigma_{ij}^{[1]} + \dot{\varepsilon}_{ij}^{[0]} \sigma_{ij}^{[0]} + \dot{\varepsilon}_{ij}^{[1]} \sigma_{ij}^{[-1]}) d\Omega - \int_{\Gamma_b} \delta \mathbf{v}^{[0]} \cdot \mathbf{h} d\Gamma \\ &\quad - \int_{\Omega} \delta \mathbf{v}^{[0]} \cdot \mathbf{b} d\Omega = 0, \end{aligned} \quad (3.16)$$

$$\begin{aligned}
I_4 = \delta \Pi_{\text{gb}}(\mathbf{v}, \bar{\mathbf{v}}) &= \int_{\Gamma_{\text{gb}}} \frac{1}{2} (\sigma_{ij}^+ \varepsilon_{ij}^+ - \sigma_{ij}^- \varepsilon_{ij}^-) \delta \bar{v}_n \, d\Gamma + \int_{\Gamma_{\text{gb}}} \gamma \left(\frac{\partial \delta \bar{v}_s}{\partial s} + \frac{\delta \bar{v}_n}{R} \right) d\Gamma \\
&+ \int_{\Gamma_{\text{gb}}} \frac{\delta \bar{v}_n}{\mu} \bar{v}_n \, d\Gamma = 0.
\end{aligned} \tag{3.17}$$

Using the chain rule $\partial(\cdot)/\partial y_i = \lambda \partial(\cdot)/\partial x_i$, the arbitrariness of $\delta v_j^{[0]}$ in Ω , and considering the symmetric stress tensor, the first leading order equation (3.14) yields the corresponding strong form:

$$\frac{1}{2} \frac{\partial}{\partial y_j} \left(C_{ijke} \left(\frac{\partial v_k^{[0]}}{\partial y_e} + \frac{\partial v_e^{[0]}}{\partial y_k} \right) \right) = 0. \tag{3.18}$$

Employing periodicity of the unit cell in Ω^y , and recasting equation (3.18) in the weak form using integration by parts in reference domain Ω^y yields

$$\frac{\partial v_i^{[0]}}{\partial y_j} = 0, \quad \Rightarrow v_i^{[0]} = v_i^{[0]}(\mathbf{x}). \tag{3.19}$$

Here it shows that the coarse scale component of the solution $v_i^{[0]}$ depends only on \mathbf{x} , and this leads to

$$\sigma_{ij}^{[-1]} = C_{ijkl} \dot{\varepsilon}_{kl}^{[-1]} = 0. \tag{3.20}$$

Similarly, by using equations (3.15) and (3.19), and employing the major symmetry of C_{ijkl} for $I_2 = 0$, we obtain the following strong form

$$\frac{\partial}{\partial y_j} [C_{ijkl} (\dot{\varepsilon}_{\bar{k}\bar{l}}^{[0]} + \dot{\varepsilon}_{\hat{k}\hat{l}}^{[1]})] = 0. \tag{3.21}$$

To satisfy equation (3.21), the fine scale material velocities should take the form of

$$v_k^{[1]} = \alpha_{kmn}(y) \dot{\varepsilon}_{\bar{m}\bar{n}}^{[0]}(x), \tag{3.22}$$

where α_{imn} is a scale coupling function. Using the scale coupling relationship in equation (3.22), the strain rate can be rewritten as

$$\dot{\varepsilon}_{\hat{i}\hat{j}}^{[1]} = \frac{1}{2} \left(\frac{\partial v_i^{[1]}}{\partial y_j} + \frac{\partial v_j^{[1]}}{\partial y_i} \right) = \dot{\varepsilon}_{\bar{m}\bar{n}}^{[0]} \eta_{ijmn}, \quad \eta_{ijmn} = \frac{1}{2} \left(\frac{\partial \alpha_{imn}}{\partial y_j} + \frac{\partial \alpha_{jmn}}{\partial y_i} \right). \tag{3.23}$$

Substitution of equation (3.23) into equation (3.21) produces the following scale-coupling equation defined in Ω^y with periodic boundary conditions

$$\frac{\partial}{\partial y_j} [C_{ijkl} (I_{klmn} + \eta_{klmn})] = 0, \quad I_{klmn} = \frac{1}{2} (\delta_{km} \delta_{ln} + \delta_{kn} \delta_{lm}). \tag{3.24}$$

The coupling function α_{imn} can be solved by a Galerkin approximation of the weak form of equation (3.24), where an integration by parts and unit cell periodicity in equation (3.24) are employed. Next, by introducing the integration of the coarse scale problem ($I_3 = 0$) over Ω^y [10], the scale coupling relationship in equation (3.23), unit cell periodicity and the coarse scale conditions in equations (3.19) and (3.20), the following strong form of homogenized coarse scale equilibrium equation is obtained

$$\begin{aligned}
\bar{C}_{ijkl} \frac{\partial \dot{\varepsilon}_{\bar{k}\bar{l}}^{[0]}}{\partial x_j} + b_i &= 0 && \text{on } \Omega^y \\
\sigma_{ij}^{[0]} n_j - h_i &= 0 && \text{on } \Gamma_h^y,
\end{aligned} \tag{3.25}$$

where \bar{C}_{ijkl} represents the homogenized constitutive tensor of C_{ijkl} in the grain structure

$$\bar{C}_{ijmn} = \frac{1}{S} \int_{\Omega^y} C_{ijkl} (I_{klmn} + \eta_{klmn}) d\Omega. \quad (3.26)$$

In response to the coarse and fine scale driving forces associated with the strain energy density jump $(\sigma^+ : \varepsilon^+ - \sigma^- : \varepsilon^-)/2$ across the grain boundary, the grain boundary velocity \bar{v} can be expressed in the form of asymptotic expansion, i.e.

$$\bar{v}_i(\mathbf{x}, \mathbf{y}) = \bar{v}_i^{[0]}(\mathbf{x}, \mathbf{y}) + \lambda \bar{v}_i^{[1]}(\mathbf{x}, \mathbf{y}) + O(\lambda^2), \quad (3.27)$$

where $\bar{v}_i^{[0]}$ and $\bar{v}_i^{[1]}$ are the coarse and fine scale components of \bar{v}_i , respectively. Substituting the expansion equations (3.27), (3.6) and the expanded strain and stress in equations (3.8) and (3.11) into equation (3.17), the following decomposed grain boundary evolution equations ($I_4 = 0$) can be obtained

$$\int_{\Omega^y} \frac{1}{2} [\varepsilon_{ij}^{+[0]} \sigma_{ij}^{+[0]} - \varepsilon_{ij}^{-[0]} \sigma_{ij}^{-[0]}] \delta \bar{v}_n^{[0]} d\Gamma + \int_{\Gamma_{gb}^y} \gamma \left(\frac{\partial \delta \bar{v}_s^{[0]}}{\partial s} + \frac{\delta \bar{v}_n^{[0]}}{R} \right) d\Gamma + \int_{\Gamma_{gb}^y} \frac{\delta \bar{v}_n^{[0]}}{\mu} \bar{v}_n^{[0]} d\Gamma = 0,$$

$$\int_{\Omega^y} \frac{1}{2} [\varepsilon_{ij}^{+[0]} \sigma_{ij}^{+[1]} + \varepsilon_{ij}^{+[1]} \sigma_{ij}^{+[0]} - \varepsilon_{ij}^{-[0]} \sigma_{ij}^{-[1]} - \varepsilon_{ij}^{-[1]} \sigma_{ij}^{-[0]}] \delta \bar{v}_n^{[1]} d\Gamma + \int_{\Gamma_{gb}^y} \frac{\delta \bar{v}_n^{[1]}}{\mu} \bar{v}_n^{[1]} d\Gamma = 0. \quad (3.28)$$

These two equations will be used to solve coarse and fine scale components of the grain boundary migration velocity. Further, the stationary conditions in equation (3.28) result in the strong forms of driving force equilibrium acting on the grain boundaries.

4. Numerical procedures for multi-scale modelling of stress grain growth

4.1. Approximation functions

The coupling functions α_{kmn} between the coarse and fine material velocities governed by the scale-coupling equation (3.24) are determined by the material properties and their distributions following the topology of grain structures. Solving the scale-coupling equation (3.24) by the conventional finite element method requires a continuous remeshing in the event of grain boundary topological changes and the evolution of grain structures. Alternatively, a moving least-square reproducing kernel (MLS/RK) approximation with grain boundary interface enrichment [9] has been introduced in the modelling of stressed grain growth process. In this work, the scale-coupling functions α_{kmn} defined in the grain domains are approximated by the MLS/RK approximation [4, 27], whereas the grain boundary velocity \bar{v} on the grain boundaries is approximated by the finite elements as

$$\alpha_{kmn}(\mathbf{y}) = \sum_{l=1}^{Nmp} \Psi_l(\mathbf{y}) \alpha_{kmnl}, \quad m, n, k = 1, 2, \quad \mathbf{y} \in \Omega^y, \quad (4.1)$$

$$\bar{v}_i^{[0]}(s) = \sum_{l=1}^{Ngbp} \bar{N}_l(s) \bar{v}_{iI}^{[0]}, \quad \bar{v}_i^{[1]}(s) = \sum_{l=1}^{Ngbp} \bar{N}_l(s) \bar{v}_{iI}^{[1]}, \quad s \in \Gamma_{gb}^y, \quad (4.2)$$

where Nmp is the number of discrete points in grain domains Ω^y , $Ngbp$ is the number of discrete points on grain boundaries Γ_{gb}^y , Ψ_l is the MLS/RK shape function [4, 8, 27], and $\bar{N}_l(s)$ is the one-dimensional finite element shape function defined along the grain boundary using grain boundary coordinate shown in figure 13(a).

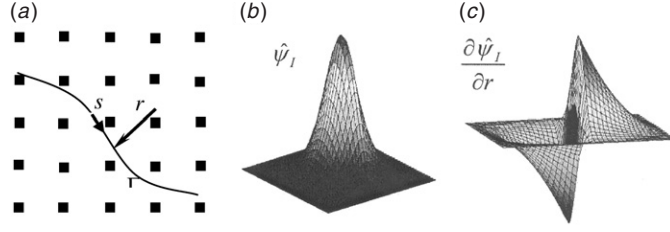


Figure 13. (a) Local coordinates of the discretized material interface. (b) Interface enrichment function. (c) Derivative of the interface enrichment function.

Due to discontinuity of material properties across the grain boundaries the MLS/RK shape function Ψ_I , used for approximating the scale-coupling functions α_{kmn} , is constructed following the grain boundary enriched reproducing kernel approximation [44] as

$$\Psi_I(\mathbf{y}) = \begin{cases} \hat{\psi}_I(\mathbf{y}), & \text{for nodes with } \mathbf{y}_I \in \Gamma_{\text{gb}} \\ \mathbf{H}^T(\mathbf{y} - \mathbf{y}_I) \mathbf{M}^{-1}(\mathbf{y}) \left[\mathbf{H}(0) - \sum_{I: \mathbf{x}_I \in \Gamma_{\text{gb}}} \hat{\psi}_I(\mathbf{y}) \mathbf{H}(\mathbf{y} - \mathbf{y}_I) \right] \\ \Phi_a(\mathbf{y} - \mathbf{y}_I), & \text{otherwise} \end{cases} \quad (4.3)$$

$$\mathbf{H}^T(\mathbf{y} - \mathbf{y}_I) = [1, y_1 - y_{1I}, y_2 - y_{2I}] \quad (4.4)$$

$$\mathbf{M}(\mathbf{y}) = \sum_{I=1}^{N_{\text{mp}}} \mathbf{H}(\mathbf{y} - \mathbf{y}_I) \mathbf{H}^T(\mathbf{y} - \mathbf{y}_I) \Phi_a(\mathbf{y} - \mathbf{y}_I), \quad (4.5)$$

where Φ_a is the cubic B-spline function with support size ‘ a ’, and $\hat{\psi}_I$ is the interface enrichment function introducing a discontinuous derivative in the r -direction:

$$\hat{\psi}_I(\mathbf{x}(r, s)) = \phi(r)\varphi(s). \quad (4.6)$$

Here the function $\phi(r)$ has a discontinuous derivative across the interface and $\varphi(s)$ is a smooth function along the interface. This interface enrichment function is defined locally on the interface with r and s being the local coordinates perpendicular to and along the interface, respectively, as shown in figure 13(a). The interface enrichment function $\hat{\psi}_I$ and its derivative are depicted in figures 13(b) and (c). Note that unlike the previous work by Moes *et al* [32] where additional degrees of freedom have been introduced to the enrichment functions on the material interfaces, the present approach does not require additional degrees of freedom for imposing interface discontinuities. This advantage becomes important when many material interfaces exist in the grain network.

At the triple junction, the enrichment function $\phi(r)$ is constructed as

$$\phi(\mathbf{r}) = \phi(r_1) + \phi(r_2) + \phi(r_3) + \phi(r_1)\phi(r_2) + \phi(r_2)\phi(r_3) + \phi(r_1)\phi(r_3) + \phi(r_1)\phi(r_2)\phi(r_3), \quad (4.7)$$

where r_1, r_2, r_3 are the local coordinates of the three grain boundaries forming the triple junction.

4.2. Discrete equations

The scale-coupling function α_{kmn} is obtained by solving the following weak form of equation (3.24)

$$\int_{\Omega^y} \beta_{imn} \frac{\partial}{\partial y_j} [C_{ijkl}(I_{klmn} + \eta_{klmn})] d\Omega = 0, \quad (4.8)$$

where β_{imn} is a weight function. Employing the integration by parts and periodicity to the pervious equation yields

$$\int_{\Omega^y} \beta_{imn,j} C_{ijkl} \eta_{klmn} \, d\Omega = - \int_{\Omega^y} \beta_{imn,j} C_{ijmn} \, d\Omega. \quad (4.9)$$

By approximating α_{kmn} using equation (4.1), the vector form of η_{klmn} in equation (3.23) can be expressed as

$$\boldsymbol{\eta} = \sum_{I=1}^r \mathbf{G}_I \boldsymbol{\alpha}_I, \quad (4.10)$$

where

$$\boldsymbol{\eta}^T = [\eta_{1111}, \eta_{1122}, \eta_{1112}, \eta_{2211}, \eta_{2222}, \eta_{2212}, 2\eta_{1211}, 2\eta_{1222}, 2\eta_{1212}] \quad (4.11)$$

$$\mathbf{G}_I = \begin{bmatrix} \Psi_{I,1} \mathbf{I} & \mathbf{0} \\ \mathbf{0} & \Psi_{I,2} \mathbf{I} \\ \Psi_{I,2} \mathbf{I} & \Psi_{I,1} \mathbf{I} \end{bmatrix}, \quad \Psi_{I,i} = \frac{\partial \Psi_I}{\partial y_i} \quad (4.12)$$

$$\boldsymbol{\alpha}_I = \begin{bmatrix} \alpha_{1I} \\ \alpha_{2I} \end{bmatrix}, \quad \boldsymbol{\alpha}_{1I} = \begin{bmatrix} \alpha_{111I} \\ \alpha_{122I} \\ \alpha_{112I} \end{bmatrix}, \quad \boldsymbol{\alpha}_{2I} = \begin{bmatrix} \alpha_{211I} \\ \alpha_{222I} \\ \alpha_{212I} \end{bmatrix}. \quad (4.13)$$

Here \mathbf{I} and $\mathbf{0}$ are 3×3 identity and zero matrices, respectively. Substituting equations (4.10)–(4.13) into equation (4.9) yields the following discretization equation:

$$\mathbf{P} \boldsymbol{\alpha} = \mathbf{q} \quad (4.14)$$

where

$$\mathbf{P}_{IJ} = \int_{\Omega^y} \mathbf{G}_I^T \mathbf{C} \mathbf{G}_J \, d\Omega \quad (4.15)$$

$$\mathbf{q}_I = - \int_{\Omega^y} \mathbf{G}_I^T \boldsymbol{\Sigma} \, d\Omega \quad (4.16)$$

$$\mathbf{C} = \begin{bmatrix} C_{1111} \mathbf{I} & C_{1122} \mathbf{I} & C_{1112} \mathbf{I} \\ C_{2211} \mathbf{I} & C_{2222} \mathbf{I} & C_{2212} \mathbf{I} \\ C_{1211} \mathbf{I} & C_{1222} \mathbf{I} & C_{1212} \mathbf{I} \end{bmatrix} \quad (4.17)$$

$$\boldsymbol{\Sigma}^T = [C_{1111}, C_{1122}, C_{1112}, C_{2211}, C_{2222}, C_{2212}, C_{1211}, C_{1222}, C_{1212}]. \quad (4.18)$$

Upon obtaining the scale-coupling function α_{kmn} , the homogenized material-constitutive tensor \bar{C}_{ijkl} can be obtained by employing equation (3.26). The coarse scale material velocity $\mathbf{v}^{[0]}$ then is solved using the homogenized equation (3.25). After solving $\mathbf{v}^{[0]}$, the fine scale material velocity $\mathbf{v}^{[1]}$ is obtained using the coupling equation (3.22). Using $\mathbf{v}^{[0]}$ and $\mathbf{v}^{[1]}$, the strain rate $\dot{\boldsymbol{\epsilon}}$, stress $\boldsymbol{\sigma}$ and strain energy density jump can be computed. By introducing approximation functions in equation (4.2) into the decomposed grain boundary evolution equation (3.28), the coarse and fine scale grain boundary velocities $\bar{\mathbf{v}}^{[0]}$ and $\bar{\mathbf{v}}^{[1]}$ are solved:

$$\mathbf{C}^{\text{gb}} \bar{\mathbf{v}}^{[0]} = -\mathbf{f}^{\text{gb}} - \mathbf{f}^{\text{st}[0]} \quad (4.19)$$

$$\mathbf{C}^{\text{gb}} \bar{\mathbf{v}}^{[1]} = -\mathbf{f}^{\text{st}[1]}, \quad (4.20)$$

where

$$\mathbf{C}_{IJ}^{\text{gb}} = \sum_{i=1}^{\text{NGB}} \int_{\Gamma_{\text{gb}(i)}^y} \frac{1}{\mu} \bar{\mathbf{N}}_I^T \mathbf{R}_n^T \mathbf{R}_n \bar{\mathbf{N}}_J \, ds \quad (4.21)$$

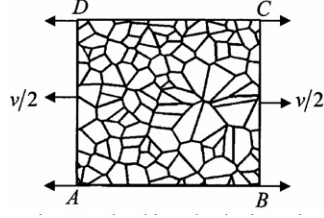


Figure 14. Unit cell of a grain network subjected to horizontal velocity (v : horizontal velocity).

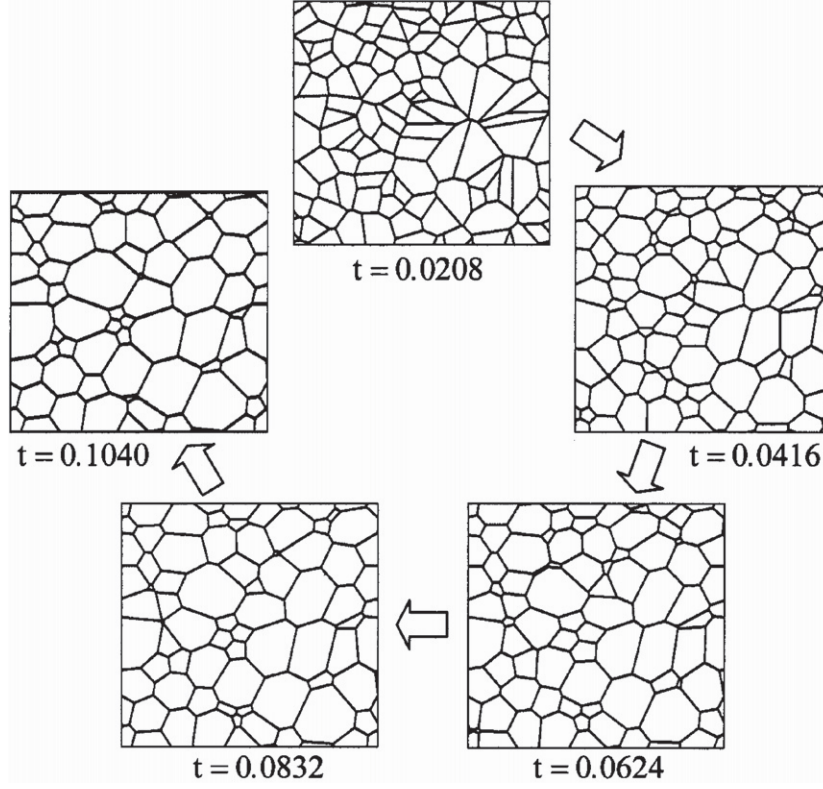


Figure 15. Grain growth evolution (t : time (s)).

$$\mathbf{f}_I^{\text{gb}} = \sum_{i=1}^{\text{NGB}} [\gamma \bar{\mathbf{N}}_I^T \mathbf{R}_s^T]_{s_i^y}^2 + \sum_{i=1}^{\text{NGB}} \int_{\Gamma_{\text{gb}(i)}^y} \gamma \frac{\bar{\mathbf{N}}_I^T \mathbf{R}_n^T}{R} ds \quad (4.22)$$

$$\mathbf{f}_I^{\text{st}[0]} = \sum_{i=1}^{\text{NGB}} \int_{\Gamma_{\text{gb}(i)}^y} \frac{1}{2} (\varepsilon_{ij}^{+[0]} \sigma_{ij}^{+[0]} - \varepsilon_{ij}^{-[0]} \sigma_{ij}^{-[0]}) \bar{\mathbf{N}}_I^T \mathbf{R}_n^T d\Gamma \quad (4.23)$$

$$\mathbf{f}_I^{\text{st}[1]} = \sum_{i=1}^{\text{NGB}} \int_{\Gamma_{\text{gb}(i)}^y} \frac{1}{2} (\varepsilon_{ij}^{+[0]} \sigma_{ij}^{+[1]} + \varepsilon_{ij}^{+[1]} \sigma_{ij}^{+[0]} - \varepsilon_{ij}^{-[0]} \sigma_{ij}^{-[1]} - \varepsilon_{ij}^{-[1]} \sigma_{ij}^{-[0]}) \bar{\mathbf{N}}_I^T \mathbf{R}_n^T d\Gamma \quad (4.24)$$

$$\bar{\mathbf{N}}_I = \begin{bmatrix} \bar{N}_I & 0 \\ 0 & \bar{N}_I \end{bmatrix} \quad (4.25)$$

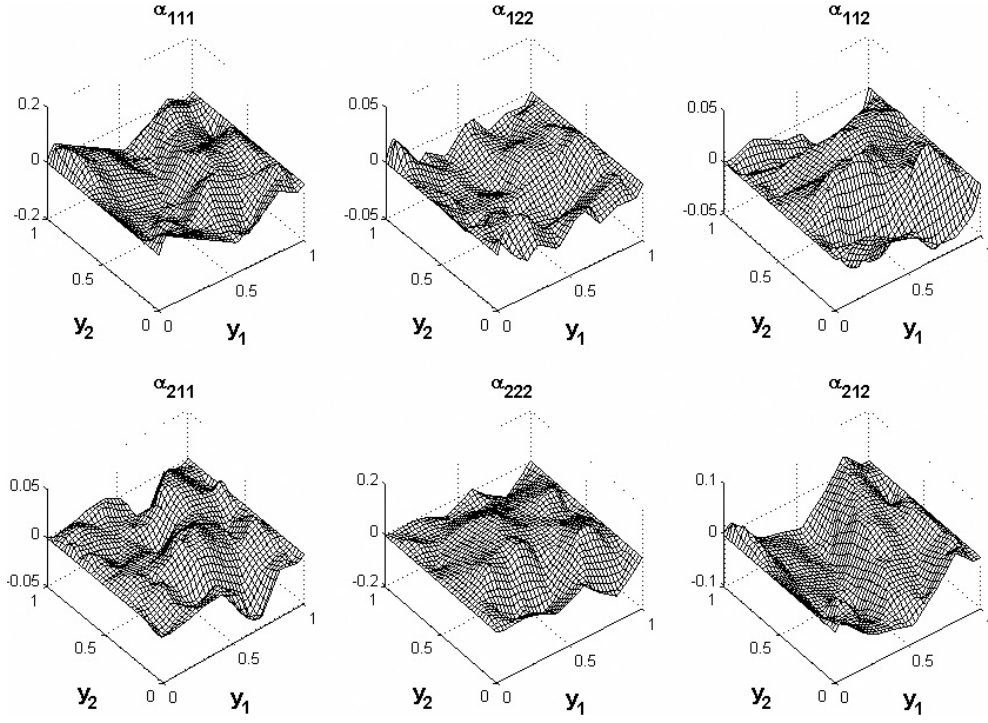


Figure 16. Coupling functions at the final stage of grain evolution.

$$\mathbf{R}_n = [e_{nx} \quad e_{ny}] \quad (4.26)$$

$$\mathbf{R}_s = [e_{sx} \quad e_{sy}], \quad (4.27)$$

where e_s and e_n are unit vectors along and normal to the boundary element, \bar{N}_i is a FE-shaped function defined on the grain boundary, s_i^1 and s_i^2 are the two end points on the GB segment i , and NGB is the number of grain boundary segments. At each time step, the coupling function is obtained from (4.14), followed by coarse and fine scale material velocities using (3.25) and (3.22), respectively. Further, the grain boundary network under material deformation is updated. Equations (4.19) and (4.20) then are solved for the grain boundary migration velocity based on the deformed grain network, which again updates the grain network.

4.3. Numerical example

Consider a grain network as shown in figure 14 subjected to uniform horizontal velocity on edges AD and BC, while the other sides CD and AB are traction free. Each grain is assumed to follow the anisotropic creep law in equation (3.5) with random orientations. Periodic boundary conditions are imposed on the boundary of the unit cell.

In this analysis, unit cell dimension is $1 \mu\text{m} \times 1 \mu\text{m}$, grain boundary properties are $\mu = 0.1 \mu\text{m} \mu\text{N}^{-1} \text{s}^{-1}$, $\gamma_b = 0.5 \mu\text{N} \mu\text{m}^{-1}$, orthotropic Young's modules are $E_1 = 3 \times 10^5 \mu\text{N} \mu\text{m}^{-2}$ and $E_2 = 6 \times 10^5 \mu\text{N} \mu\text{m}^{-2}$, the applied horizontal velocity is $50 \mu\text{m} \text{s}^{-1}$, and time step size is $\Delta t = 0.0004 \text{s}$. Uniform discrete points of 60×60 for interface-enriched MLS/RK approximations of scale-coupling function are employed, and each segment of grain boundaries is discretized by six finite element points. The grain structure evolution modelled

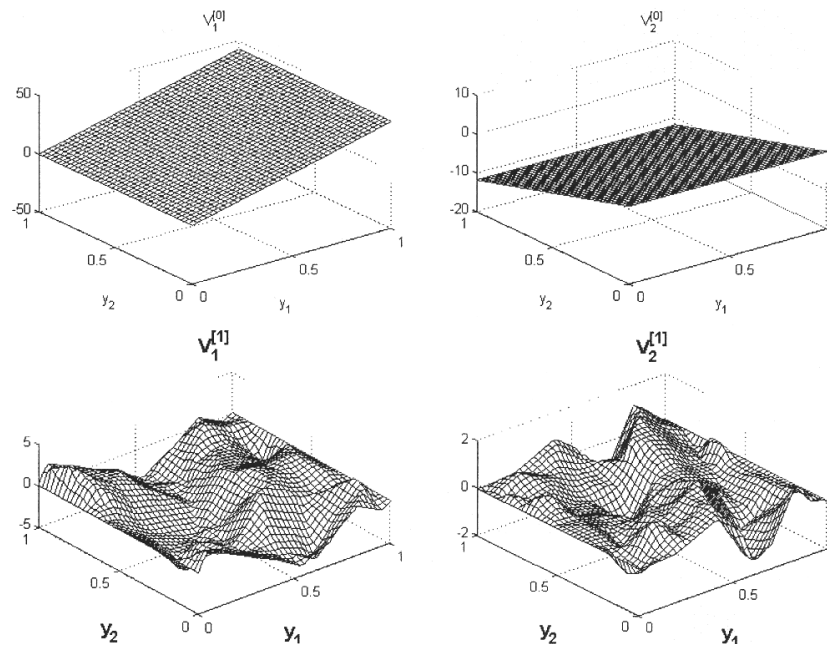


Figure 17. Coarse and fine scale material velocities at the final stage of grain evolution.

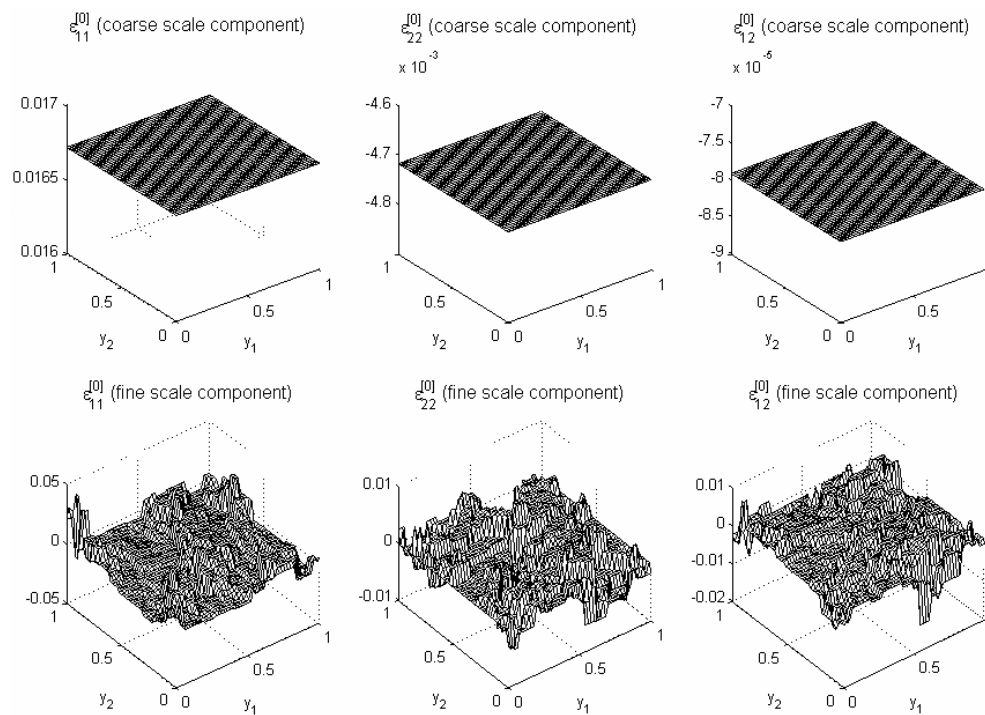


Figure 18. Coarse and fine scale strains at the final stage of grain evolution.

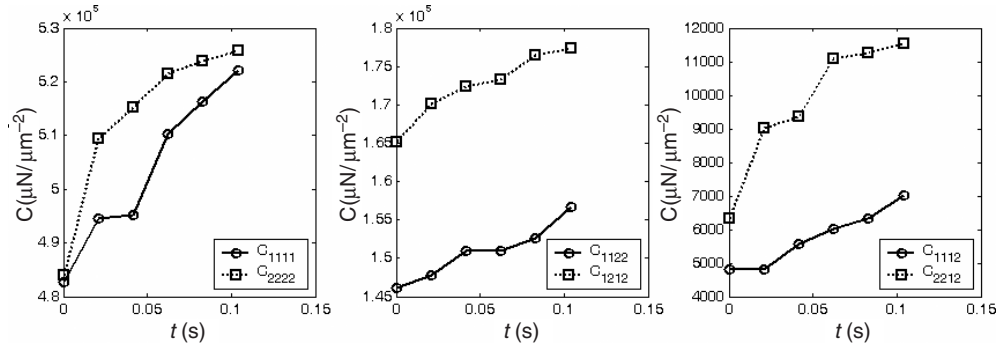


Figure 19. Evolution of homogenized material properties during the grain structure evolution.

by the proposed multi-scale method is shown in figure 15. The spatial distribution of the scale-coupling functions α_{ijk} at $t = 0.104$ s are plotted in figure 16. Using α_{ijk} , the coarse and the fine scale material velocity are obtained and plotted in figure 17. Coarse and fine scale strains for the last stage also are presented in figure 18. Note that the macroscopic (coarse scale) strain rate at a point in macroscopic coordinate \mathbf{x} is a constant function in the \mathbf{y} coordinate in the mesoscopic level unit cell, whereas the mesoscopic (fine scale) strain displays fluctuations in the \mathbf{y} coordinate due to the inhomogeneities in the unit cell. The homogenized material constants \bar{C}_{1111} , \bar{C}_{2222} , \bar{C}_{1122} , \bar{C}_{1112} , \bar{C}_{2212} and \bar{C}_{1212} at a few selected configurations are shown in figure 19. Note that the material constants increase as the microstructures evolve for two reasons: (1) in order to reduce total free energy, the grains with lower strain energy density are forced to grow, while the ones with higher strain energy density are forced to shrink; and (2) the strain energy density in a grain under deformation is inversely proportional to the rigidity of the grain. These phenomena are shown in figure 19, where the homogenized grain structure becomes stiffer as grains evolve.

5. Conclusions

In this paper we presented two classes of multi-scale methods, one based on the employment of multi-scale scaling and wavelet basis functions for solving problems with fixed microstructures, and the other based on asymptotic expansion with a special discretization technique for modelling problems with evolving microstructures.

In the first part of this work, a multi-scale wavelet Galerkin homogenization method was proposed for homogenization of heterogeneous materials with fixed microstructures. The linear orthogonal scaling function and wavelet were constructed and utilized as shape functions under the wavelet Galerkin framework. The corresponding transformation matrix also was constructed for efficient up- and down-scaling operations. Compared to the widely used Haar basis, the proposed linear orthogonal scaling function and wavelet are capable of capturing a more localized response. The use of a linear orthogonal scaling function and a wavelet avoids the difficulty of missing data near the boundaries when Haar bases are used. Further, the employment of these functions in the wavelet Galerkin formulation with the consideration of integration by parts, yields a symmetric system with a lower order of differentiation.

Several enhancements were proposed to resolve difficulties encountered in the wavelet Galerkin method for multi-scale homogenization. First, the wavelet Galerkin approach leads to a singular stiffness matrix due to dependency of the linear scaling functions and wavelets between any two adjacent discrete points. To remove this singularity, a zero energy mode

shifting method was introduced. Another difficulty associated with wavelet-based multi-scale homogenization is the loss of accuracy in the boundary conditions during the homogenization process. To correct this deficiency, a mirror image technique utilizing the property that the wavelet projection filters out the deviation from the average was proposed.

A major restriction of the wavelet Galerkin method for multi-scale homogenization is that it requires a uniform grid at the finest scale. This presents complexity in multi-dimensional heterogeneous media with irregular-shaped microstructures, where the interface cannot be discretized properly with a uniform grid. To resolve this difficulty, a wavelet projection method was proposed. In this approach, the fine scale solution can be obtained by any kind of numerical method, and the method is not confined to inhomogeneous media with regular-shaped microstructures. To correctly interpolate information at the boundaries during the process of homogenization, the mirror image technique also has been utilized in this approach. By means of wavelet transformation based on linear orthogonal scaling functions and wavelets, the decomposition of high and low scale solution components at any scale can be carried out effectively.

The wavelet-based methods that rely on fixed grid points to obtain the finest scale solution become ineffective for problems involving microstructure evolution and moving interfaces. In the second part of this paper, a method based on an asymptotic expansion of a variational equation in conjunction with a double-grid numerical method was introduced for multi-scale modelling and homogenization of problems with evolving microstructures. To yield a variationally consistent multi-scale formulation, a variational equation based on the principle of virtual power was adopted. The field variables were expressed in the form of asymptotic expansion to yield the leading-order equations in the expanded variational equation. This approach yields multi-scale Euler equations representing grain structure equilibrium and grain boundary evolution equations on meso- (fine) and macro- (coarse) scale levels, and also yields the scale-coupling relationship. The scale-coupling function between coarse and fine material velocities allows a dynamic down-scaling (homogenization) and up-scaling (localization) as the microstructure evolves. To solve the scale-coupling function numerically, a double-grid discretization was employed. This double-grid method allows arbitrary evolution of microstructure topology. The grain boundary jump conditions also were handled properly by the interface enrichment functions. The proposed formulation was applied to multi-scale modelling and homogenization of stressed grain growth. The effect of grain growth process on the homogenized elasticity tensor also was characterized.

Acknowledgment

The support of this work by NSF under grant CMS 0084589 to the University of California, Los Angeles is greatly appreciated.

Appendix A. Orthogonal scaling and wavelet functions

A multi-resolution analysis makes use of a function ϕ and a nested sequence of closed subspaces $\{V_j\}_{j \in \mathbb{Z}}$ in which each subspace is related to its next finer subspace through the scaling law:

$$\phi(x) \in V_j \Leftrightarrow \phi(2x) \in V_{j+1}, \quad j \in \mathbb{Z}. \quad (\text{A.1})$$

The translates of $\phi(x)$ span the same subspace, i.e.

$$\phi(x) \in V_0 \Leftrightarrow \phi(x - n) \in V_0, \quad \text{for all } n \in \mathbb{Z}. \quad (\text{A.2})$$

Hence any function in V_0 can be expressed in terms of the basis functions of V_1 , i.e.

$$\phi(x) = \sum_{n=-\infty}^{\infty} a_n \phi(2x - n), \quad (\text{A.3})$$

where a_n are given values for each particular function $\phi(x)$, referred to as the ‘scaling function’.

The orthonormal complement of V_{j-1} in V_j , W_{j-1} , is defined for any $j \in \mathbb{Z}$, $j > i$,

$$\begin{aligned} V_j &= V_i \oplus \left(\bigoplus_{k=0}^{j-i-1} W_{i+k} \right) \\ \bigoplus_{j \in \mathbb{Z}} W_j &= L^2(\mathbb{R}). \end{aligned} \quad (\text{A.4})$$

By imposing orthogonality conditions [11], orthonormal wavelet basis functions can be obtained

$$\psi_{j,n}(x) = 2^{j/2} \psi(2^j x - n), \quad n, j \in \mathbb{Z}. \quad (\text{A.5})$$

These wavelet functions $\psi_{j,n}(x)$ constitute an orthonormal basis for W_j . By virtue of (A.4), the wavelet function $\psi(x)$ can be expressed in terms of the scaling function $\phi(x)$ at the next finer scale:

$$\psi(x) = \sum_{n=-\infty}^{\infty} b_n \phi(2x - n). \quad (\text{A.6})$$

An orthogonal scaling function with respect to translation now can be constructed by the Fourier transform of the following relationship

$$\phi(x) = \sum_n c_n \sqrt{2} \phi(2x - n), \quad n \in \mathbb{Z}, \quad (\text{A.7})$$

where c_n are given for any particular scaling function. For an arbitrary scaling function ϕ (candidate function), the orthogonal scaling function ϕ^* can be represented by moving the candidate function along the x -axis:

$$\phi^*(x) = \sum_n \alpha_n \phi(x - n), \quad (\text{A.8})$$

in which α_n are obtained through imposing the orthogonality condition in the Fourier space. The orthogonal wavelet function then can be constructed by applying the Fourier transform to the two scale relation in equation (A.6) to yield

$$\psi^*(x) = \sqrt{2} \sum_{-n-1} (-1)^{n-1} d_{-n-1} \sum_m \alpha_m \phi(2x - m - n), \quad (\text{A.9})$$

where d_{-n-1} are the wavelet coefficients which can be obtained by taking the Fourier transform of equations (A.6) and (A.7). The procedures for construction of the piecewise linear orthogonal scaling and wavelet function shown in figure 1 can be found in [11]. Once we have the orthogonal scaling and wavelet functions constructed, we can utilize them as shape functions in the wavelet Galerkin method.

Appendix B. Transformation matrices for Haar basis and linear basis

The discrete operators P_j and Q_j for the Haar basis and the wavelet transformation operator w_j take the form of

$$P_j = \frac{1}{\sqrt{2}} \begin{bmatrix} 1 & 1 & 0 & 0 & \cdots & 0 & 0 \\ 0 & 0 & 1 & 1 & \cdots & 0 & 0 \\ \vdots & \vdots & \vdots & \vdots & \cdots & \vdots & \vdots \\ 0 & 0 & 0 & 0 & \cdots & 1 & 1 \end{bmatrix}_{2^{j-1} \times 2^j},$$

$$\mathbf{Q}_j = \frac{1}{\sqrt{2}} \begin{bmatrix} 1 & -1 & 0 & 0 & \cdots & 0 & 0 \\ 0 & 0 & 1 & -1 & \cdots & 0 & 0 \\ \vdots & \vdots & \vdots & \vdots & \cdots & \vdots & \vdots \\ 0 & 0 & 0 & 0 & \cdots & 1 & -1 \end{bmatrix}_{2^{j-1} \times 2^j} \quad (\text{B.1})$$

$$\mathbf{w}_j = \begin{bmatrix} \mathbf{Q}_j \\ \mathbf{P}_j \end{bmatrix} = \frac{1}{\sqrt{2}} \begin{bmatrix} 1 & -1 & 0 & 0 & \cdots & 0 & 0 \\ 0 & 0 & 1 & -1 & \cdots & 0 & 0 \\ \vdots & \vdots & \vdots & \vdots & \cdots & \vdots & \vdots \\ 0 & 0 & 0 & 0 & \cdots & 1 & -1 \\ 1 & 1 & 0 & 0 & \cdots & 0 & 0 \\ 0 & 0 & 1 & 1 & \cdots & 0 & 0 \\ \vdots & \vdots & \vdots & \vdots & \cdots & \vdots & \vdots \\ 0 & 0 & 0 & 0 & \cdots & 1 & 1 \end{bmatrix} \quad (\text{B.2})$$

For the linear scaling function and wavelet, the discrete transformation operators \mathbf{P}_j and \mathbf{Q}_j can be written as

$$\mathbf{P}_j = \begin{bmatrix} a_{j-2k} & 0 & 0 & 0 & 0 & \cdots \\ a_{j-2(k+1)} & a_{j+1-2(k+1)} & a_{j+2-2(k+1)} & 0 & 0 & \cdots \\ a_{j-2(k+2)} & a_{j+1-2(k+2)} & a_{j+2-2(k+2)} & a_{j+3-2(k+2)} & a_{j+4-2(k+2)} & \cdots \\ \vdots & \vdots & \vdots & \vdots & \vdots & \vdots \\ 0 & 0 & 0 & 0 & 0 & \cdots \\ 0 & 0 & 0 & 0 & 0 & \cdots \\ & 0 & 0 & 0 & 0 & \\ & 0 & 0 & 0 & 0 & \\ & \vdots & \vdots & \vdots & \vdots & \\ a_{j+m-2-2(k+n-1)} & a_{j+m-1-2(k+n-1)} & a_{j+m-2(k+n-1)} & & & \\ 0 & 0 & a_{j+m-2(k+n)} & & & \end{bmatrix} \quad (\text{B.3})$$

$$\mathbf{Q}_j = \begin{bmatrix} b_{j-2k} & 0 & 0 & 0 & 0 & \cdots \\ b_{j-2(k+1)} & b_{j+1-2(k+1)} & b_{j+2-2(k+1)} & 0 & 0 & \cdots \\ b_{j-2(k+2)} & b_{j+1-2(k+2)} & b_{j+2-2(k+2)} & b_{j+3-2(k+2)} & b_{j+4-2(k+2)} & \cdots \\ \vdots & \vdots & \vdots & \vdots & \vdots & \vdots \\ 0 & 0 & 0 & 0 & 0 & \cdots \\ 0 & 0 & 0 & 0 & 0 & \cdots \\ & 0 & 0 & 0 & 0 & \\ & 0 & 0 & 0 & 0 & \\ & \vdots & \vdots & \vdots & \vdots & \\ b_{j+m-2-2(k+n-1)} & b_{j+m-1-2(k+n-1)} & b_{j+m-2(k+n-1)} & & & \\ 0 & 0 & b_{j+m-2(k+n)} & & & \end{bmatrix} \quad (\text{B.4})$$

and the corresponding transformation matrix takes the form of

$$w_j = \begin{bmatrix} Q_j \\ P_j \end{bmatrix}, \quad (\text{B.5})$$

where k , n and m are specified from the non-zero coefficients of the sequence a_i and b_i [11], and j is the level of resolution.

References

- [1] Amaratunga K, William J and Yokoyama S 1992 Wavelet based hierarchical solutions of partial differential equations *Proc. Complas III, 3rd Int. Conf. on Computational Plasticity, Fundamentals and Applications (Barcelona, Spain, April 1992)*
- [2] Babuska L 1975 Homogenization and its applications *Technical Note* B. N. 821
- [3] Bakhvalov N S and Panasenko G P 1984 *Homogenization of Periodic Medium Process* (Moscow: Nauka)
- [4] Belytschko T, Lu Y Y and Gu L 1994 Element-free Galerkin methods *Int. J. Numer. Methods Eng.* **37** 229–56
- [5] Benssousan A, Lions J L and Papanicoulau G 1978 *Asymptotic Analysis for Periodic Structures* (Amsterdam: North Holland)
- [6] Boggess A and Narcowich F J 2001 *A First Course in Wavelets with Fourier Analysis* (Englewood Cliffs, NJ: Prentice Hall)
- [7] Brewster M and Beylkin G 1995 A multiresolution strategy for numerical homogenization *Appl. Comput. Harmon. Anal.* **2** 327–49
- [8] Chen J S, Han W, You Y and Meng X 2003 A reproducing kernel method with nodal interpolation property *Int. J. Numer. Methods Eng.* **56** 935–60
- [9] Chen J S, Kotta V, Lu H, Wang D, Moldovan D and Wolf D 2004 A variational formulation and a double-grid method for meso-scale modeling of stressed grain growth in polycrystalline materials *Comput. Methods Appl. Mech. Eng.* **193** 1277–303
- [10] Chen J S and Mehraeen S 2004 Variationally consistent multiscale modeling and homogenization of stressed grain growth *Comput. Methods Appl. Mech. Eng.* **193** 1825–48
- [11] Chen J S and Mehraeen S 2004 Wavelet Galerkin method in multi-scale homogenization of heterogeneous media *Int. J. Numer. Methods Eng.* accepted
- [12] Christensen R M 1990 A critical evaluation for a class of micromechanics models *J. Mech. Phys. Solids* **38** 379–404
- [13] Chui C K 1992 *An Introduction to Wavelets* (New York: Academic)
- [14] Coult N A 1997 A multi-resolution strategy for homogenization of partial differential equations *PhD Thesis*, Department of Applied Mathematics, University of Colorado
- [15] Dahlke S and Weinreich I 1993 Wavelet-Galerkin methods: an adapted biorthogonal wavelet basis *Constr. Approx.* **9** 237–62
- [16] Dahmen W, Kurdila A and Oswald P 1997 *Multiscale Wavelet for Partial Differential Equations (Wavelet Analysis & its Applications)* (San Diego: Academic)
- [17] Daubechies I 1992 Ten lectures on wavelets (CBMS-NSF Series in *Appl. Math.* **61** Philadelphia: SIAM)
- [18] Dorobantu M and Engquist B 1998 Wavelet-based numerical homogenization *J. Numer. Anal.* **35** 540–59
- [19] Duvaut G 1976 *In Theoretical and Applied Mechanics* (Amsterdam: North-Holland)
- [20] Fish J and Belsky V 1995 Multi-grid method for periodic heterogeneous media, 1-Convergence studies for one-dimensional media *Comput. Methods Appl. Mech. Eng.* **126** 1–16
- [21] Fish J and Shek K 2000 Multi-scale analysis of composite materials and structures *Compos. Sci. Technol.* **60** 2547–56
- [22] Glowinski R, Lawton W, Ravachol M and Tenenbaum E 1990 Wavelet solution of linear and nonlinear elliptic, parabolic, and hyperbolic problems in one space dimension *Proc. 9th Int. Conf. on Numerical Methods in Applied Sciences and Engineering* (Philadelphia: SIAM)
- [23] Hill R 1963 Elastic properties of reinforced solids: some theoretical principles *J. Mech. Phys. Solids* **11** 357–72
- [24] Hori M and Nemat-Nasser S 1999 On two micromechanics theories for determining micro–macro relations in heterogeneous solids *Mech. Mater.* **31** 667–82
- [25] Knappek S 1996 Matrix-dependant multi-grid homogenization for diffusion problems *J. Sci. Comput.* **20** 515–33
- [26] Lato A, Resnikoff H and Tenenbaum E 1992 The evaluation of the connection coefficients of compactly supported wavelets *Proc. French–USA Workshop on Wavelets and Turbulence (Princeton University, June 1991)* (Berlin: Springer)

- [27] Liu W K, Jun S, Li S, Adee J and Belytschko T 1995 Reproducing kernel particle methods for structural dynamics *Int. J. Numer. Methods Eng.* **38** 1655–79
- [28] Liu W K, Hao W, Chen Y, Jun S and Gosz J 1997 Multiresolution reproducing kernel particle methods *Comput. Mech.* **20** 295–309
- [29] Liu W K, Chen Y, Chang C T and Belytschko T 1996 Advances in multiple scale kernel particle methods *Comput. Mech.* **18** 73–111
- [30] Mehraeen S and Chen J S 2004 Wavelet-based multi-scale projection method in homogenization of heterogeneous media *J. Finite Element Anal. Des.* **40** 1665–79 (Finalist of Robert Melosh student paper competition, 2004)
- [31] Mignot F, Puel J-P and Suquet P-M 1980 Homogenization and bifurcation of perforated plates *Int. J. Eng. Sci.* **18** 409–14
- [32] Moes N, Dolbow J and Belytschko T 1999 A finite element method for crack growth without remeshing *Int. J. Numer. Methods Eng.* **46** 131–50
- [33] Morral J E and Ashby M F 1974 Dislocated cellular structures *Acta Metall.* **22** 567–75
- [34] Moulinec M and Suquet P 1998 A numerical method for computing the overall response of nonlinear composites with complex microstructure *Comput. Methods Appl. Mech. Eng.* **157** 69–94
- [35] Mura T 1987 *Micromechanics of Defects in Solids* (Dordrecht: Martinus Nijhoff)
- [36] Nemat-Nasser S 1993 Bounds and estimates of overall moduli of composites with periodic microstructure *Mech. Mater.* **15** 163–81
- [37] Nemat-Nasser S 1999 Averaging theorems in finite deformation plasticity *Mech. Mater.* **31** 493–523
- [38] Nemat-Nasser S and Hori M 1993 *Micromechanics: Overall Properties of Heterogeneous Solids* (Amsterdam: Elsevier)
- [39] Nemat-Nasser S and Hori M 1995 Universal bounds for overall properties of linear and nonlinear heterogeneous solids *J. Eng. Mater. Technol.* **117** 412–32
- [40] Qian S and Weiss J 1993 Wavelets and the numerical solution of partial differential equations *J. Comput. Phys.* **106** 155–75
- [41] Sanchez-Palencia E and Zaoui A 1985 *Homogenization Techniques for Composites, Homogenization Techniques for Composite Media* (Berlin: Springer)
- [42] Vaithyanathan V, Wolverton C and Chen L Q 2002 Multi-scale modeling of precipitate microstructure evolution *Phys. Rev. Lett.* **88** 125503-1–4
- [43] von Neumann J 1952 *Discussion Remark Concerning Paper of C S Smith, Grain Shapes and Other Metallurgical Applications of Topology* (Cleveland, Ohio: American Society for Metals) pp 108–10
- [44] Wang D and Chen J S 2002 Homogenization of magnetostrictive particle-filled elastomers using meshfree method with interface discontinuity *J. Finite Element Anal. Des.* **39** 765–82 (Finalist of Robert Melosh student paper competition, 2002)
- [45] Weiss J 1991 Wavelet and the study of two dimensional turbulence *Proc. French–USA Workshop on Wavelets and Turbulence* (Princeton University, June 1991) ed Y Maday (New York: Springer)
- [46] Yu Q and Fish J 2002 Multi-scale asymptotic homogenization for multi-physics problems with multiple spatial and temporal scales: a coupled thermo-viscoelastic example problem *Int. J. Solids Struct.* **39** 6429–52